SAND2014-17487J

Mechanical and Functional Behavior of High Temperature Ni-Ti-Pt Shape Memory Alloys

T.E. Buchheit, J.E. Massad, D.F. Susan, J.R. McElhanon
Sandia National Laboratories
Albuquerque, NM 87185

R.D. Noebe
NASA Glenn Research Center
Cleveland, OH 44135

Abstract

Alloying NiTi SMAs with Pt at the expense of Ni has been shown to increase the temperature required to induce the martensite-austenite transformation up to 1000°C. Due to a focus on achieving high transformation temperatures, studies of Ni-Ti-Pt alloys have dealt primarily on alloys with relatively high Pt concentrations, i.e., ≥ 20 at.%. In an effort to identify alloys suitable for application as a thermal fail-safe device, e.g., that undergo transformations between 175°C and 225°C with recoverable shape memory strains greater than 2%, a series of Ti-rich Ni-Ti-Pt ternary alloys with 13 – 18 at.% Pt were processed by vacuum arc melting and characterized for their transformation behavior in the homogenized condition. The phase transformation temperatures determined by DSC correlated well with interpolated results from previous studies. From this broader set of compositions three alloys containing 15.5 - 16.5 at.% Pt exhibited transformation temperatures in the vicinity of 200°C. For these three targeted compositions, preliminary microstructural evaluation showed a martensitic microstructure with only small amounts of $Ti_2(Ni,Pt)$ particles. Room-temperature tensile testing of martensite showed de-twinning stress in the 130-180 MPa range, ultimate strengths of 500-600 MPa, and 7-9% elongation to failure. Elevated temperature tests in austenite displayed yield stress of approximately 500 MPa and 3.5% elongation to failure. The strain recovery in tension was investigated with unbiased strain-temperature tests of incremental prestrain from 1-5%, as well as cyclic strain-temperature testing at 3% prestrain. The unbiased shape recovery results indicated a complicated strain recovery path, dependent on prestrain level, but overall, acceptable SMA behavior for the targeted application.

Introduction

The temperature at which the reversible martensite-austensite transformation occurs in a shape memory alloy defines the operational range of its key unique behaviors, the shape memory effect (SME) and superelasticity. The upper limit for the transformation temperatures of the most commercially successful shape memory alloys (SMAs), derived from near equiatomic Ni-Ti compositions, is approximately 100°C. Exploiting the shape memory effect and superelasticity characteristics of these alloys for engineering applications is therefore restricted to temperatures near that limit. As opportunities to utilize the unique properties of SMAs continue to expand, developing alloys with increased transformation temperature has become an area of active research for commercial, aerospace, and defense applications.[1] Replacement of nickel by either platinum or palladium in binary NiTi alloys has been shown to elevate the martensitic transformation temperature and, therefore, the operational temperature range of the shape memory response in these alloys, but only after a critical level of either Platinum group metal is added.[1-4] In the case of replacing Ni with Pt, the onset of increasing transformation temperature occurs beyond 10 at% Pt and the phase transformation temperature can be increased to as high as 1000ºC with complete replacement of Ni with Pt.[2-4]

For both Ni-Ti-Pt and Ni-Ti-Pd compositions, the high temperature austenite phase maintains a B2 crystal structure even after complete substitution of Ni with Pt or Pd. However, at certain percentages of the alloying element, whether Pd or Pt, the martensite structure changes from B19′ (monoclinic) martensite, associated with near equiatomic NiTi, to a B19 (orthorhombic) martensite structure. In Ni-Ti-Pt alloys, the change in this crystallographic aspect of the transformation occurs near 5 - 10% Pt. However, an exact association between the change in martensitic crystal structure and a shift toward increasing transformation temperature with platinum content has not been established.[1,3]

As Pt is added to Ni-Ti alloys, the ductility decreases, as demonstrated by the room temperature tensile properties of Ni-Ti-Pt alloys reported by Hosoda and coworkers.[5] In particular, reported results just above the target compositions of the present investigation show room temperature tensile ductility between 1-4% for Ni-Ti-Pt compositions ranging between 20-30 at.% Pt.[5-7] These values are significantly less than tensile ductility values reported for binary NiTi SMAs, which can be greater than 20%. However, with proper thermomechanical

processing, tensile ductilities on the order of 10% and fracture strengths exceeding 1 GPa are possible.[8]

Reported recoverable strain due to the phase transformation, i.e. shape memory strains, in Ni-Ti-Pt alloys containing 20 at.% Pt range between 1% - 2.5% in the stress free condition after tensile loading.[3] Load biased shape memory experiments suggest that these strains could perhaps be increased through training to about 4% in alloys with similar compositions.[6,9] This is comparable to binary NiTi with similar microstructure (e.g., near equiaxed grain structure and random texture),[10] but less than recoverable strains commonly obtained in highly textured commercial grade binary Ni-Ti compositions, which can approach 8-9%.[11] Load biased shape memory experiments on Ni-Ti-Pt alloys also suggest that (Ni,Pt)-rich compositions exhibit better reversibility and dimensional stability than Ti-rich compositions, but much smaller recoverable strains.[12]

Unlike many other applications of SMAs, where multiple actuation cycles are of interest, the mechanical testing in this work focused on the characteristics important for a thermal fail-safe device (one time use or a limited-cycle actuation) in an abnormal thermal environment. Abnormal temperature sensing would be required, for example, in an accidental fire scenario, outside of ambient operating, storage, and manufacturing conditions and for our purposes would be about 200ºC. To this end, a range of compositions containing between 13 at.% Pt and18 at.% Pt were fabricated and their phase transformation characteristics were assessed using differential scanning calorimetry (DSC). Three compositions with a transformation temperature close to 200ºC on heating and otherwise favorable characteristics suggested by the DSC traces were selected for further testing. Their nominal Pt content ranged between 15.5 at.% - 16.5 at.%. The mechanical properties and shape memory behavior of these compositions were investigated with a miniature custom high temperature mechanical test system using small tensile coupons machined from arc-melted ingots. With regard to the previous understanding of the SMA characteristics of Ni-Ti-Pt alloys, mechanical testing in this investigation focused on interrogating the following traits: shape memory strain, low and high temperature ductility, suppression of any two-way shape memory effect, and preliminary measurements of the cyclic shape memory behavior and stability. Cursory microstructural characterization was also conducted primarily to characterize the martensitic structure and identify any additional phases that may be present in the microstructures. A distinguishing feature of this investigation into the

shape memory behavior of Pt bearing NiTi-based alloys relative to previous studies is the current focus on alloys with transformation temperatures near 200°C, while previous studies have emphasized compositions with higher Pt concentrations and transformation temperatures >250°C.[3,6,8,12]

Experimental Procedures

Material Processing and Characterization

A series of $Ni_{49.5-x}$-$Ti_{50.5}$-Pt_x alloys with Pt concentrations between 13 and 18 at.% were prepared for this investigation by vacuum arc-melting of pure elemental constituents in a small arc button melter equipped with a water cooled copper crucible. The ingots were remelted at least two times, and as many as four times, flipping the ingot between each remelt. The final cast ingots were homogenized in a vacuum furnace at 1050°C for 60 hours. The homogenization step encourages a uniform Pt concentration within the cast dendritic structure of the ingots and has been found to be critical for obtaining good shape memory behavior in the alloys.

Differential scanning calorimetry (DSC) was performed using a TA Instruments Q200 differential scanning calorimeter to determine stress-free phase transformation temperatures. A series of $Ni_{49.5-x}$-$Ti_{50.5}$-Pt_x alloys with Pt contents from 13 at.% to 18 at.% Pt were analyzed and compared to the previously published data on Ni-Ti-Pt SMAs. Small samples for DSC analysis were cut with a slow-speed diamond wafering saw from the interior of the ingots. The DSC analyses were carried out across a temperature range from room temperature to 300°C with heating and cooling rates of 10°C/min. Austenite-start (A_s) and austenite-finish (A_f) temperatures on heating and the martensite-start (M_s) and martensite-finish (M_f) temperatures on cooling were determined by the baseline tangent method.[13] Multiple heating and cooling cycles (3-5) were performed with the DSC instrument to determine the stability of the phase transformation behavior of each sample.

Samples from the homogenized ingots for microstructural characterization were mounted in cold-setting epoxy, ground, and polished with standard metallographic techniques. The martensitic microstructure was analyzed in a Zeiss Supra 55VP SEM equipped with an Oxford/HKL electron backscatter diffraction (EBSD) system with Channel 5 software. Large precipitates, found along prior austenite grain boundaries as well as within grains, were

characterized by energy dispersive spectroscopy (EDS). The materials in this study were targeted to be slightly Ti-rich (~50.5 at.% Ti) so fine-scale precipitation associated with Ni-rich binary Ni-Ti and ternary Ni-Ti-Pt alloys was not anticipated.[14-17]

Mechanical Testing

Small rectangular (1.55 mm wide, 0.2 mm thick) mechanical test samples with a 7.9 mm gage length were electro-discharge machined (EDM) from the homogenized ingots. An EDM tensile sample compared to the original arc melt ingot is shown in Fig. 1(a). The test samples were lightly sanded with 600 grit paper to remove the EDM re-cast layer. However, subsequent SEM characterization revealed that some of the residual re-cast layer remained on the surface of the test specimens. After EDM machining and prior to mechanical testing, the samples were heated above the A_f temperature in a flat configuration to set their initial shape. The small-scale tension testing was performed using a custom tabletop servohydraulic load frame similar to the system described in ref. [18]. The test frame was designed to characterize the room temperature and high temperature properties of small specimens and was ideally suited for testing the small EDM'd SMA samples. An Interface Inc. 100 lb. load cell was used to measure load in all tensile tests. To measure displacement, the frame was fitted with a Keyence Corp. LS5041R high speed laser micrometer with 1 μm resolution. To accommodate temperature, the test system was fitted with a clamshell furnace with slits allowing the laser to pass through the furnace for the displacement measurement of the gage section of the sample. Small tabs were gently spot-welded near the ends of the sample gage section for the laser extensometer measurement. Sample temperature was measured using thermocouple leads placed in the fillet region very close to the gage section. Figure 1(b) shows a sample mounted and gripped in the test system and includes portions of the grips and opened clamshell furnace, illustrating how test specimen gage displacement and temperature were measured during the experiments.

Mechanical testing included baseline isothermal tension testing in the martensitic and austenitic states and strain-temperature cycling under load-free conditions to characterize the shape memory behavior. The loading portions of the experiments were stroke controlled with an effective strain rate of 4×10^{-4} s^{-1}. Mechanical test results presented in this study are always reported for a given temperature. While this temperature is representative of the actual

temperature in the center of the gage section, the samples had an approximately 10°C-15°C temperature gradient along their gage length due to thermal sinking from the grips.

Results

Differential Scanning Calorimetry (DSC)

Figure 2 shows characteristic DSC traces for the three selected alloys in the 15.5-16.5 at.% Pt range. The DSC traces displayed slightly different transformation temperatures for the first heating cycle but all cooling cycles and subsequent heating cycles were identical. To highlight the transformation temperature shift observed after the first thermal cycle in each result presented in Figure 2, the first cycle is indicated by a dashed curve and subsequent cycles are solid lines. Additional cycles after the second exhibited no additional shift in phase transformation temperatures, thus a temperature stabilized phase transformation response was achieved by the second cycle in all cases.

The transformation on heating is due to the martensite to austenite transformation, from which the austenite start and finish temperatures, A_s and A_f, were extracted as illustrated in Fig. 2(a). Similarly, the austenite to martensite transformation temperatures, M_s and M_f, were obtained from the cooling cycle trace also illustrated in Fig 2(a). Table I lists the transformation temperatures after stabilization for the three selected alloys whose DSC traces are shown in Fig. 2. In each case, both the forward and reverse phase transformations occurred over approximately a 20°C span, defined by the peak width. The hysteresis between the heating and cooling transformations, defined by the difference between A_f and M_s temperatures, was narrow (~14 °C) by comparison with binary Ni-Ti alloys, which generally display hysteresis of 30 °C or greater.[10,11]

The summary plots in figure 3 show the M_s and A_s transformation temperatures as a function of nominal at.% Pt taken from the DSC results of all thirteen compositions across the 13 at.% Pt – 18 at.% Pt range. Results from several previously reported transformation temperature measurements across the entire range of possible compositions in the Ni-Ti-Pt system, i.e. $Ni_{50-x}Ti_{50}$-Pt_x where $0 < x < 50$ provide a trend line that can be used for comparison.[1-4] The trend line is plotted for M_s as a function of at.% Pt in both plots in Figure 3. Although it is taken from a less populated data set across a wide range of compositions, the results from within the narrow

range of compositions targeting the 200°C transformation in this study fit well with the interpolated curve. The reverse transformation, where an SMA structure would actuate under a predefined abnormal high temperature event, for example, drives a specific interest in the A_s temperature for alloy design. Because the hysteresis is small in these alloys across the 10 at.% Pt – 20 at.% Pt range (a result originally reported by Rios et al. [2]), the M_s temperatures are very similar to the observed A_s temperatures as clearly shown in Fig. 3(b). Thus, the same trend line seems a useful guide for identifying alloy compositions designed for an A_s temperature requirement.

Mechanical Behavior

A. Tensile Behavior of the Martensite and Austenite Phases

To evaluate the basic mechanical properties of the cast and homogenized martensite and austenite phases, multiple specimens from each of the three selected alloy compositions spanning the 15.5 at.% -16.5 at.% Pt range (listed in Table I) were tested in tension at room temperature (R.T.) and at 275°C. Figure 4 shows examples of the resulting stress strain curves. At R.T., well below A_s for these alloys, the material is expected to be fully martensitic. Four representative stress-strain curves from the three compositions tested at R.T. are shown in figure 4(a), two are included for the 15.5 at.% composition to demonstrate the possible variation in samples tested from the same ingot. The results show an appreciable plateau region, with a plateau range between 3%-5% strain, attributed to mechanically driven de-twinning and reorientation of martensite variants. The stress at which martensite de-twinning begins to dominate the mechanical response of the alloys, i.e. the de-twinning stress, σ_{dt}, is characterized by the "knee" in the stress-strain curves. It ranged between 130 and 180 MPa across the compositions tested. There appeared to be a weak correlation in the de-twinning stress with Pt content, with the de-twinning stress tending to increase with Pt level.

Figure 4(b), tests performed at 275°C, well above A_s, shows the stress-strain behavior for each alloy in its fully austenitic (B2 crystal structure) state. As expected, the austenitic material behaves like a “typical” metal alloy exhibiting an elastic region followed by plastic yielding, deformation, and failure. The yield strength of all three alloys was approximately 500 MPa and the samples exhibited 3-4% elongation to failure in the austenite phase. Compared to the room temperature martensitic response of the material, the stress-strain curves show nearly identical

behavior across the range of alloys tested. The lesser degree of scatter among the tests is attributed to the isotropic behavior of the cubic austenite phase, even though the same small sample size and large grain size (relatively few grains tested) were still a constraint in these tests (see Fig. 5 below). The results also indicate a relatively insensitive effect of Pt content on sample strength over the narrow range of Pt contents investigated (15.5 -16.5%). The behavior displayed in figure 4(b) was also comparable to that observed by Noebe et al.[6] for the 20at.% Pt alloy, that is, a 400-500 MPa yield strength at 300-330°C.

The degree of variability in tensile behavior at R.T. between samples from the same ingot is demonstrated by the stress-strain curves shown in figure 5. In this figure, stress-strain curves are shown for three 16% Pt alloy tensile specimens, figure 5(a), and three 16.5% Pt alloy tensile specimens, figure 5(b), are shown. Rather than testing to failure, these samples were tested to a strain between 0.05-0.08 (5%-8%), unloaded and heated above the A_f temperature to thermally recover the de-twinned martensite. Recovery of all the applied strain, except less than 0.01 (1%), was observed in all samples. Other than to demonstrate thermal recovery of the applied strains, the intent of these experiments was to determine the degree of variability in the shape of the stress-strain curves for samples tested through the plateau region but not to final failure. The variation is attributed to the small-size specimens, the relatively large prior austenite grain size across the gage section, and the highly orientation dependent behavior of the low-symmetry martensitic phase. The results highlight the importance of testing multiple samples when sub-size tensile coupons are used to evaluate cast/homogenized material with relatively large grain size.

For specimens tested at R.T., figures 4(a) and 5, as the de-twinning process (plateau region) completes, the martensite sustains additional deformation at a high hardening rate. Final fracture (figure 4 only) occurs at stress levels between 500 and 700 MPa. For comparison, previous tension test results on similar Ni-Ti-Pt compositions are included as dashed gray lines in figure 4. The curves are from a 15at% Pt alloy [7] and two 20at% Pt alloys [6,7]. For those materials, the de-twinning plateaus were not as pronounced or absent. A key difference is that those materials were hot worked after the casting and homogenization treatments. Specifically, Noebe et. al. extruded their cast ingots at 1100°C and Takahashi et al. hot forged their alloys at temperatures between 1000°C-1400°C depending on the composition. In addition, the tests in the referenced studies were performed on larger samples with a different geometry, both of which could affect the ease of propagation of a transformation front responsible for the plateau

region. Therefore, while the *apparent* ductility is about 3% higher for the samples in the present study (3-6% for [6] and [7] compared to 6-9% here), the difference can likely be attributed to the plateau behavior stabilized by the small sample size and rectangular geometry used in this investigation. Furthermore, the variability in final fracture strain depends on the extent of the plateau region. Subsequent shape memory experiments demonstrated that the Noebe et al. 20 at.% Pt alloy did exhibit strain recovery up to 3-4%, the full extent of the stress-strain curve shown in Figure 4. Takahashi et al.[7] also reported perfect shape memory recovery of their 15 at% Pt composition after 3% tensile strain. Both results suggest that although a stress-plateau was not prominent or even evident, de-twinning still occurred to an extent similar to that observed for the compositions in this study.

B. Shape Memory Behavior: Stress-Strain-Temperature Response

Two types of experiments were performed to characterize the unconstrained shape memory behavior of the three selected alloys. i) Thermal shape recovery tests with increasing incremental strain between cycles and ii) Cyclic shape recovery tests to 3% strain. The first series of experiments were used to determine the amount of tensile strain the materials can recover after deformation at room temperature via unconstrained heating (under zero applied stress). The second series of tests were used to determine the evolution of the recovery process with repeated straining to a constant applied strain and thermal cycling. To shape-set the samples before testing, they were heated to 275°C in a flat configuration and furnace cooled. The incremental shape recovery experiments consisted of straining the samples at room temperature to 1%, followed by a complete unload, then a zero load heat to recovery (A_f + 30°C), and cool to room temperature. Total applied strain was then incremented by an additional 1% at room temperature (referencing from the *initial* sample gage length) so that the sample was strained 2% followed by same recovery procedure, i.e. unload, heat to recovery, cool to room temperature. On the third cycle the sample was strained to 3% followed by the same recovery procedure etc. This experiment was repeated increasing the strain by another 1% for each cycle until 5% total strain was achieved. Thus, the completed test was composed of five incrementally increasing strain and thermal recovery cycles. Stress-strain results and corresponding strain-temperature results from these tests are shown in Figure 6.

In the cyclic shape recovery experiments, specimens were strained to 3% and thermally recovered ten times to determine the cyclic stability of these compositions. The 3% strain level was chosen based on analysis of the shape recovery results and was referenced to the initial sample gage length and original cycle. Between each cycle, samples were unloaded, heated through the recovery temperature (at least $A_f + 30°C$), held at that temperature for 5 minutes, and then cooled to room temperature. The entire process was then repeated 10 times. The stress-strain results and corresponding strain-temperature results from these experiments are shown in Figure 7.

Both experiments characterize the strain recovery associated with the martensite to austenite transformation after initial deformation (reorientation and de-twinning) of the martensite at room temperature. The strain-temperature plots (Figs. 6 and 7) show that the specimens recover most of the inelastic strain induced at room temperature as they transform to austenite between 200°C – 230°C, consistent with the DSC temperatures listed in Table I. Strain recovery during the martensite to austenite transformation during the cyclic shape recovery experiments (Fig. 7) resulted in transformation strains in the range of 1%-1.5%. In the higher prestrain cycles of the incremental shape recovery experiments (Fig. 6), transformation strains of ~1.5% to greater than 3% were achieved, depending on the initial applied strain.

While slight differences in stress-strain behavior might be expected with changes in Pt composition, the differences in the stress-strain response in the plateau regime observed among the different samples tested and shown in figures 6 and 7, such as the initial de-twinning stress and initial slope of the plateau, were again attributed to the small sample sizes and small number of grains within the gage section. Another feature of note in figure 7 is the decreasing de-twinning stress with increasing number of cycles. This behavior represents a slight “training” of the material during strain-temperature cycling. The martensite variants that form during the cooling (austenite to martensite) transformation are oriented more favorably with respect to the applied stress direction, thus de-twinning more readily when the next load is applied.

Microstructural Characterization

To support the mechanical test measurements, SEM characterization was performed on tensile test coupons from the 15.5 at.% Pt and 16.5 at.% Pt alloys. Samples were extracted from the grip and gage sections of coupons tested to failure at room temperature, representing unstrained and strained sections of material. Figure 8 shows backscatter SEM photomicrographs from both the grip and gage sections of a tested 15.5 at.% Pt tensile coupon. Mechanical testing results, discussed above, showed that martensite de-twinning and variant reorientation are the primary deformation modes in these alloys at room temperature. The martensitic microstructure is evident along with micron-sized precipitates with darker contrast, likely formed during ingot casting and possibly coarsened during homogenization. At higher magnification in the grip section, Figure 8(b), martensite variants are readily observable and appear to be highly twinned, as expected. In the gage section images, there is some possible evidence of de-twinned regions within the microstructure, as suggested in Figure 8(d).

Using EDS, the micron-sized precipitates were found to be Ti-rich and Ni-lean relative to the matrix. Based on this work and other characterization studies, the precipitates were tentatively identified as $Ti_2(Ni,Pt)$, similar to those identified by Rios et al. and Noebe and coworkers.[2,6,8] Electron backscatter diffraction (EBSD) also confirmed the cubic crystal symmetry of the precipitate phase consistent with the $Ti_2(Ni,Pt)$ crystal structure.

Discussion

A. Tensile Response of Martensitic and Austenitic Phases of the Ni-Ti-Pt HTSMA

Compared to binary Ni-Ti SMA compositions, replacing Pt with Ni in the 10at%-20at% range significantly reduces the tensile ductility, particularly in the austenite phase. However, the results also suggested that cast + homogenized alloys, with relatively clean microstructures (only small amounts of micron-sized $Ti_2(Ni,Pt)$ particles) exhibit comparable plastic ductility at room temperature to hot worked Ni-Ti-Pt alloys. Hot working, however, is likely to produce a more consistent mechanical response due to grain refinement and elimination of gross variations in the as-cast microstructure. The cast + homogenized microstructure is not necessarily ideal nor representative of a finished component formed into its final geometry (wire, sheet, etc.). However, the coarse microstructure and the presence of micron-size precipitates did not seem to

negatively affect the ductility or expected shape memory behavior since the cast + homogenized material exhibited shape recovery comparable to previously demonstrated hot worked alloys with similar composition.

The relatively high strain to failure observed in the room-temperature experiments (compared to past studies of NiTiPt [6,7]) can be partly attributed to the plateau-like behavior, which was probably promoted by the small number of martensite variants tested and the thin rectangular geometry of the tensile samples leading to a Luders' type propagation of the de-twinning process. In addition, the fact that these alloys were prepared by arc melting and not induction melting using a graphite crucible, a common processing route for larger batches of Ti-rich alloys, eliminated the presence of carbides in the microstructure. This may have led to a slightly higher ductility than otherwise expected for the compositions studied in this investigation.

B. Interpretation of the Shape Recovery Results

Inspection of the individual cycles from the incremental shape recovery and cyclic recovery experiments, focusing on the strain vs. temperature response, revealed three general types of behaviors. Examples of each are given in Figure 9. To characterize the evolving HTSMA behavior obtained from the experiments, the individual cycles were parameterized as shown in the figure, extracting several strain measures using an intersecting tangent technique as illustrated in the plots. Figures 9(a-c) display three different types of behavior for three different applied prestrain levels, starting with the highest strain behavior in Fig. 9a, which is discussed first. A similar evolution in strain-temperature response was observed with increasing cycle count during the cyclic recovery tests at 3% strain. The evolution in strain-temperature response is nearly saturated at the conclusion of either the incremental shape recovery or the cyclic recovery tests, thus a description of Figure 9 best begins by describing the response near the end of those experiments. Thus, a cycle near the end of a shape recovery experiment is shown in Figure 9(a), then progressing backwards in cycles or strain to an intermediate cycle in Figure 9(b), and finally to the first cycle in a shape recovery experiment shown in Figure 9(c).

Figure 9(a) shows the strain vs. temperature curve for test cycle #5 for the Ni-Ti-16.0% Pt alloy, strained to 5% at room temperature. This curve is representative of a nearly saturated response observed in all three alloys after several cycles during the cyclic recovery experiments

(Fig. 7) or after applied strains of at least 0.04 (4%) in the incremental shape recovery experiments (Fig. 6). Several measures of strains occurring during the cycle, i.e. net strain, transformation strain, TWSME (two-way shape memory effect) strain etc., are graphically identified in Figure 9(a). Some interdependence and evolution from previous cycles governs each of these strain measures. For example, since the specimen has accumulated some irrecoverable strain from the previous cycles the applied strain for a given cycle is referenced back to the original sample length, the *total strain* applied during this cycle, as indicated on the plot, is somewhat less than the nominal value of 0.05, since there is a starting residual strain of nearly 0.01 on the sample.

After applying a given strain at room temperature, the sample is completely unloaded, prior to cycling the temperature, and experiences an *elastic recovery,* which is evident in all cycles but identified only in Figure 9(b). Upon heating, a measurable continuous shape change counter to that typically expected due to thermal expansion is defined as *'negative component of thermal expansion'*. This type of behavior has been reported previously in high temperature Ni-Ti-Pd alloys[9,22] and is contrary to a generally expected positive slope due to thermal expansion. Monroe et al.[22] suggested that this negative strain response is due to the highly anisotropic thermal expansion characteristics of the martensite phase. Although the overall volume will increase with temperature, as expected, in some directions the martensite phase will contract. Through thermomechanical cycling, certain martensite variants tend to become preferentially aligned along the test direction, which coincidently also display negative expansion characteristics, such that a linear contraction is observed during heating while the SMA is martensitic. (Note that the negative CTE is not observed on the initial low strain cycle where the martensite consists of a random self-accommodated martensite structure, Figure 9(c).) Such anisotropic behavior, including martensite variants with negative thermal expansion, has been measured in monoclinic NiTi martensite[24] and later confirmed in Ni-Ti-Pd orthorhombic martensite and other martensitic systems.[22,25]

A_s and A_f temperatures are determined using the tangent intercept method and the strain recovery that occurs between these two values is identified as the *transformation strain*. On cooling, the strain associated with the austenite to martensite transformation is identified as the *two-way shape memory effect (TWSME)* strain. Inflections in the strain-temperature curve that define this strain are sometimes distinct enough to identify M_s and M_f temperatures by the

tangent intercept method as is done in Figure 9(a). Interestingly, unlike the strain response observed on heating, the expected response due to thermal contraction (of fully accommodative martensite) was always observed on cooling between M_f and room temperature. Finally, the difference in strain between the beginning of the cycle and the end of the cycle is the *unrecovered strain*.

Figure 9(b) is taken from the Ni-Ti-15.5%Pt alloy prestrained to 3% at room temperature prior to thermal cycling. This type of response is often observed within the 2%-4% prestrain cycles, duirng the incremental shape recovery experiments (Figure 6). This behavior is also observed in the early cycles of the cyclic 3% strain tests, especially for the 15.5 at.% Pt sample (figure 7(a)). Overall, the strain-temperature response in Figure 9(b) is similar to that observed in Figure 9(a) except for the direction of the strain response during the austenite to martensite transformation on cooling, resulting in an additional increment of strain in the same direction as recovery rather than the direction of the TWSME shown in Figure 9(a). This strain is thought to be a linear manifestation of the volume change as the material naturally transforms from austenite to martensite and dominates at low prestrain or thermal cycle values.[22] Figure 9(c) shows a strain referred to as a volumetric shape change associated with a transformation from austenite to *self-accomodated martensite* and Figure 9(a) shows TWSME associated with a transformation from austenite to *internally biased martensite*. Figure 9(b) illustrates a cycle early enough in the evolutionary process that the volumetric shape change strain still dominates in the austenite to martensite transformation portion of the cycle. Figures 6 and 7 show the progression of TWSME with increasing strain and accumulated cycles, which follows previous observations on SMA's. For example, in the extreme case of ~14% tensile strain of NiTi martensite, a two-way shape memory strain of 2.2% is possible with only simple tensile deformation of the martensite phase.[23]

Finally, Figure 9(c) represents the response observed in all three compositions during the initial low strain (1% prestrain) thermal recovery experiments. The initial cycle did not exhibit a negative CTE during heating, such as that observed in Figures 9(a) and (b), because the martensite still consisted predominantly of random self-accommodated variants and was not strained enough to manifest the anisotropic CTE behavior of a few re-oriented/de-twinned martensite variants. Because the measured strains are small in this case, there are effects observed that are not usually considered during load-biased shape memory behavior or the

stress-free recovery tests of an SMA deformed to much larger strains (such as the result shown in Figure 9(a)). The applied strain and thus the degree of de-twinning and reorientation of the martensite phase are minimal, and therefore the subsequent recovered strains associated with the transformation are small. Consequently, strain recovery due to the martensite to austenite transformation is not significantly different in magnitude from the increase in strain due to the linear manifestation of the volume expansion from martensite to austenite.[22] In fact, the volume expansion strain actually dominates and there is a slight increase in strain as the material proceeds through the transformation from martensite to austenite. Generally, at these small strains, effects can also be skewed due to the anisotropic nature of the martensite. The contraction on cooling is much larger than what the average axial component of the volumetric strain would be expected, but due to the previous deformation, the martensite may contain a slightly textured or preferred orientation that maximizes strain effects in the axial direction. Although this behavior was observed for the first cycle in all three alloys, the overall strain levels are small and these effects become overwhelmed at large strain behaviors, as shown in Figure 9(a).

C. Evolution of the Shape Memory Response in the Selected Ni-Ti-Pt Alloys

With the various strains identified per Figure 9, each can be plotted as a function of total applied strain for the incremental shape recovery experiments, Figure 10, or plotted as a function of cycle number for the cyclic (3% strain) recovery experiments, Figure 11. Recall that the initial state for all specimens was a shape-set condition where the specimen was thermally cycled above A_f in a flat configuration with no applied load. Also worth noting is that both the cyclic experiments with an applied strain of 0.03 and the shape recovery experiments with incremental applied strain are no-load strain recovery experiments; the transformation is not biased with an applied load during the thermal cycle.

Starting from the initial state, behavior such as that exhibited in Figure 9(c) was observed at the 0.01 strain increment for all three alloys during the strain recovery experiments. Thus, they always exhibited a small strain in the opposite direction of the expected transformation strain on the first 0.01 strain cycle and a negative strain on cooling due to volumetric effects. To simplify the plots in Figs. 10 and 11, the volumetric strains and the TWSME strains are combined and plotted as TWSME + vol., since they are competing effects that occur as a result

of the phase transformation on cooling. As the total strain was increased on successive cycles in the incremental shape recovery experiments the TWSME component gradually increased, transitioning this strain measure from a negative (volume change dominated) to positive (TWSME dominated) value with the transition point usually occurring at an applied strain of approximately 0.03.

One of the goals of this investigation was to identify a shape recovery strategy that minimizes the impact of TWSME. Thus, the 0.03 strain value was chosen for the cyclic shape memory experiments precisely because the TWSME + vol. strain was observed to be near zero at this applied strain value in the incremental shape recovery experiments for all of the compositions (Figure 10). Indeed, Figure 11 shows that the first cycle of each cyclic experiment has a zero or slightly negative TWSME + vol. strain component. Results show that the TWSME + vol. measure did increase with cycle number, saturating to a 0.002-0.004 value by the final cycle for each composition. The TWSME + vol. saturation value seemed to be dependent on the initial value after the first cycle. For example, TWSME + vol. for the 15.5% Pt composition after the first cycle, shown in the plot given in Figure 11(a), is -0.003 and saturates to a value of 0.002 by the tenth and final cycle. TWSME + vol. for the 16.5% composition after the first cycle is only slightly negative and increases and then saturates to a larger positive value of 0.004 by the final cycle. Thus, TWSME + vol. increased by about 0.004-0.005 from its initial value after the first cycle for each composition.

In Figure 11, most if not all of the strain values stabilize after about seven cycles. The phenomenon of training/stabilization of strains in Figure 11, as well as the decrease in de-twinning stress as a function of cycles in the stress vs. strain results shown in Figures 6 and 7, suggests a progressive build-up of martensite variants with favorable orientation, i.e. biased martensite, as the material is cyclically strained after only a few cycles. Thus, the work here indicates that while the Ni-Ti-Pt in this study does not demonstrate perfect SMA behavior (realizing some unrecovered strain per cycle), it does exhibit reasonable SMA behavior, requiring relatively little training. Thus, at low to moderate strain levels, these alloys are suitable for device implementation that utilizes the one-way shape memory effect and is one of only a handful of alloys capable of meeting the temperature requirement for actuation near 200°C.

Summary and Conclusions

Ternary Ni-Ti-Pt shape memory alloys with transformation temperatures near 200°C were produced and the shape memory behaviors characterized. Based on the results the following conclusions can be made.

- Ternary Ni-Ti-Pt alloys were arc melted and homogenized for 60 hours at 1050°C. Alloys with $Ni_{49.5-x}$-$Ti_{50.5}$-Pt_x, where x = 13 to 18 at.% Pt, display shape memory phase transformation temperatures covering the range 150 to 250°C. Alloys with 15.5 to 16.5 at.% Pt exhibit transformation temperatures near 200 °C. The alloy microstructures consist of lath martensite at room temperature along with a small number of micron-sized Ti_2(Ni,Pt) particles.

- Tensile testing of alloys with 15.5 to 16.5 at.% Pt at room temperature revealed de-twinning/reorientation stresses in the 130-180 MPa range, ultimate strengths of 500-650 MPa, and 7-9% elongation to failure. Variability among test results was due to the small specimen size, large prior austenite grain size, and consequently few martensite variants across the gage section of the specimens. Elevated temperature tests in austenite displayed reproducible behavior with yield stress in the vicinity of 500 MPa and approximately 3.5% elongation to failure.

- Thermal cycling of samples incrementally strained at room temperature from 1-5% resulted in good, but complicated strain recovery processes and overall reasonable SMA behavior. Additionally, small strain changes were also observed on cooling with the strain being either negative (due to volumetric changes) or positive (due to an evolving TWSME) depending on the initially applied strain level. This strain change on cooling was minimized for thermal recovery tests with 3% applied strain.

- Cyclic strain-temperature testing of samples repeatedly strained to 3%, unloaded, and thermally recovered, showed stabilization of behavior after approximately seven cycles. A slight buildup of TWSME occurs with cycling and saturates at positive values about 0.4%-0.5% greater than those measured after the initial cycle.

Acknowledgements

The authors wish to thank Mark Reece for expertise in arc button melting. Bonnie McKenzie and Alice Kilgo are acknowledged for SEM work and metallographic sample preparation. Thanks also to Don Bradley for DSC analysis, Dave Schmale for expert mechanical testing, and Dereck Johnson for the ICP analyses. Thanks to Dr. Anita Garg for helpful discussions and detailed microstructural characterization and Dr. Ken Eckelmeyer for careful review of the manuscript. RDN would like to acknowledge additional support from the NASA FAP Aeronautical Sciences Project.

References

[1] Ma J., Karaman I., and Noebe R.D.,"High temperature shape memory alloys", *International Materials Reviews*, 2010, vol. 55, no. 5, pp 257-315.

[2] Rios O., Noebe R., Biles T., Garg A., Palczer A., Scheiman D., Seifert H.J., Kaufman M.," Characterization of Ternary NiTiPt High-Temperature Shape Memory Alloys" Smart Structures and Materials 2005: Active Materials: behavior and Mechanics, SPIE Vol. 5761, ed. W.D. Armstrong, pp. 376-387.

[3] Lindquist, P.G. and Wayman, C. M., "Shape Memory and Transformation Behavior of Martensitic Ti-Pd-Ni and Ti-Pt-Ni Alloys", Engineering Aspects of Shape Memory Alloys, 1990, pp. 58-68.

[4] Takahashi Y., Tsuji M., Sakurai J., Hosada H., Wakashima K., Miyazaki S.,"Shape Memory Characteristics of TiNi-TiPt Pseudobinary Alloys", *Transactions of the Materials Research Society of Japan*, 2003, vol. 28, no. 3, pp. 627-630.

[5] Hosoda, H., Tsuji, M., Takahashi, Y., Inamura T., Wakashima K., Yamabe-Mitarai Y., Miyazaki S., and Inoue K., "Phase Stability and Mechanical Properties of Ti-Ni Shape Memory Alloys containing Platinum Group Metals", *Materials Science Forum*, 2003, Vols. 426-432, pp. 2333-2338.

[6] Noebe R., Gaydosh D., Padula II S., Garg A., Biles T., Nathal M.,"Properties and Potential of Two (Ni,Pt)Ti Alloys for use as High Temperature Actuator Materials", Smart Structures and Materials 2005: Active Materials: behavior and Mechanics, SPIE Vol. 5761, ed. W.D. Armstrong, pp. 364-375.

[7] Takahashi Y., Inamura T., Sakurai J., Hosoda H., Wakashima K., Miyazaki, S.,"Transformation behavior of Ti-Ni-Pt high temperature shape memory alloys", *Transactions of the Materials Research Society of Japan*, 2004, vol. 29, no. 7, pp. 3005-3008.

[8] R. Noebe, S. Draper, D. Gaydosh, A. Garg, B. Lerch. Nicholas, Penney, G. Bigelow, S. Padula, and J. Brown, "Effect of Thermomechanical Processing on the Microstructure, Properties, and Work Behavior of a $Ti_{50.5}Ni_{29.5}Pt_{20}$ High-Temperature Shape Memory Alloy," SMST 2006: Proceedings of the International Conference on Shape Memory and Superelastic Technologies, ASM International, Metals Park, OH., (2008), pp. 409-426.

[9] Noebe R., Padula II S., Bigelow, G., Rios, O., Garg, A., and Lerch, B.,"Properties of a Ni19.5Pd30Ti50.5 high temperature shape memory alloy in tension and compression", Smart Structures and Materials 2006: Active Materials: behavior and Mechanics, SPIE Vol. 6170, ed. W.D. Armstrong, pp. 617010-1 - 617010-13

[10] S. Padula, S. Qiu, D. Gaydosh, R. Noebe, G. Bigelow, A. Garg and R. Vaidyanathan, "Effect of Upper-Cycle Temperature on the Load-Biased, Strain-Temperature Response of NiTi," *Metallurgical & Materials Transactions*, 43A (2012) 4610-4621.

[11] Shape Memory Materials, Otsuka K., and Wayman C.M., Cambridge University Press, 1999, Chp. 10. ISBN 0521663849.

[12] Grant Hudish, Influence of Microstructure on the Shape Memory Properties of Two Ti-Lean, Ni-Ti-Pt High Temperature Shape Memory Alloys," PhD Dissertation, Colorado School of Mines, 2013.

[13] Differential Scanning Calorimetry, Hohne, G.W.H., Hemminger, W.F., and Flammersheim, H.J., Springer, Berlin, 2003, pp 116-119.

[14] Kovarik, L., Yang, F., Garg, A., Diecrks, D., Kaufman, M., Noebe, R.D., and Mills, M.J.,"Structural Analysis of a new precipitate phase in high temperature TiNiPt shape memory alloys", *Acta Materialia*, vol. 58, 2010, pp.4660-4673.

[15] Gau, Y., Zhou, N., Yang, F., Cui, Y., Kovarik, L., Hatcher, N., Noebe, R., Mills, M.J., Wang, Y., "P-phase precipitation and its effect on martensitic transformation in (Ni,Pt)Ti shape memory alloys", *Acta Materialia*, 60, 2012, pp. 1514-1527.

[16] Khalil Allafi J., Ren X., and Eggeler G., "The mechanism of multistage martensitic transformations in aged Ni-rich NiTi shape memory alloys", *Acta Materialia*, vol. 50, 2002, pp. 793-803.

[17] F. Yang, R.D. Noebe, and M.J. Mills. "Precipitates in a near-equiatomic (Ni+Pt)-rich TiNiPt alloy," *Scripta Materialia*, 69 (2013) 713-715.

[18] Buchheit T.E., LaVan D.A., Michael J.R., Christenson T.R., and Leith S.D., "Microstructural and Mechanical Properties Investigation of Electrodeposited and Annealed LIGA Nickel Structures", *Metallurgical and Materials Transactions A*, 2002, vol. 33, pp. 539-554.

[19] Jones NG, Dye D.,"Influence of applied stress on the transformation behavior and martensite evolution of a Ti-Ni-Cu shape memory alloy", *Intermetallics*, 2013, vol. 32, pp. 239-249.

[20] Mercier O. and Melton K.N.,"The Substitution of Cu of Ni in NiTi Shape Memory Alloys", *Metallurgical Transactions A*, vol. 10, 1979, pp. 387-389.

[21] H.C. Donkersloot and J.H.N. Van Vucht, "Martensitic Transformations in Gold-Titanium, Palladium-Titanium, and Platinum-Titanium Alloys near the Equiatomic Composition", *J. Less-Common Metals*, vol. 20, 1970, 83-91.

[22] Monroe JA, Karaman I, Lagoudas DC, Bigelow G., Noebe RD, and Padula II S.,"Determining recoverable and irrecoverable contributions to accumulated strain in a NiTiPd high-temperature shape memory alloy during thermomechanical cycling", *Scripta Materialia*, 2011, vol. 65, pp 123-126.

[23] O. Benafan, S.A. Padula, R.D. Noebe, T.A. Sisneros, R. Vaidyanathan, "Role of B19' martensite deformation in stabilizing two-way shape memory behavior in NiTi," *Journal of Applied Physics*, 112 (2012) 093510.

[24] S. Qiu, V.B. Krishnan, S.A. Padula, R.D. Noebe, D.W. Brown, B Clausen, R. Vaidyanathan, "Measurement of the lattice plane strain and phase fraction evolution during heating and cooling in shape memory NiTi," *Applied Physics Letters*, 95 (2009) 141906.

[25] J.A. Monroe, personal communication, Texas A&M University, (2013).

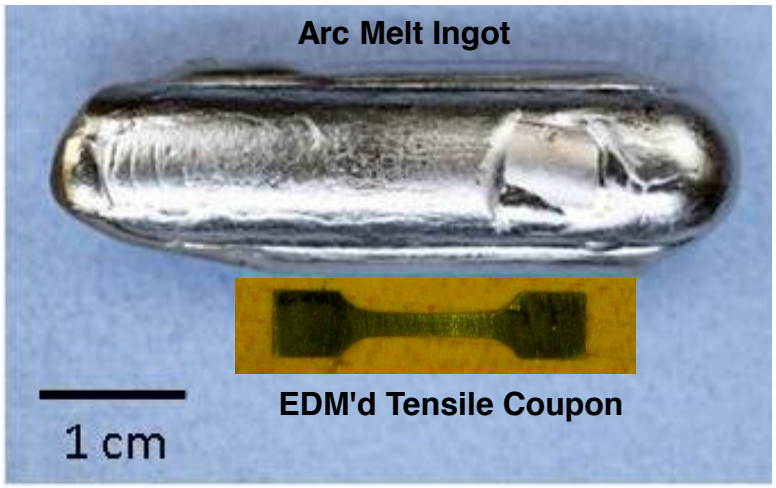

(a)

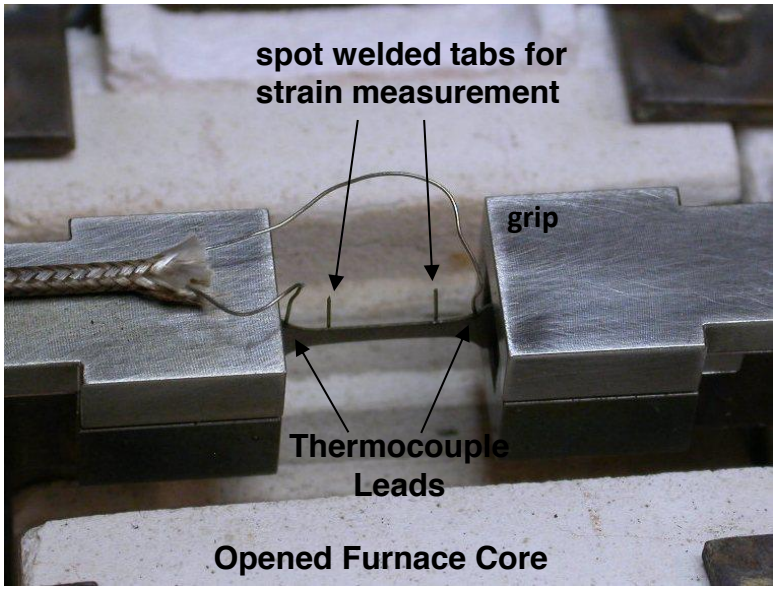

(b)

Figure 1- Photographs of (a) arc melt ingot and (b) Tensile coupon mounted in mechanical test frame.

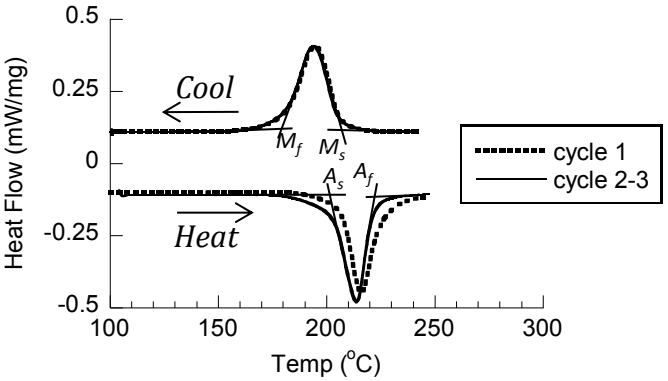

(a) 15.5%Pt (nominal)

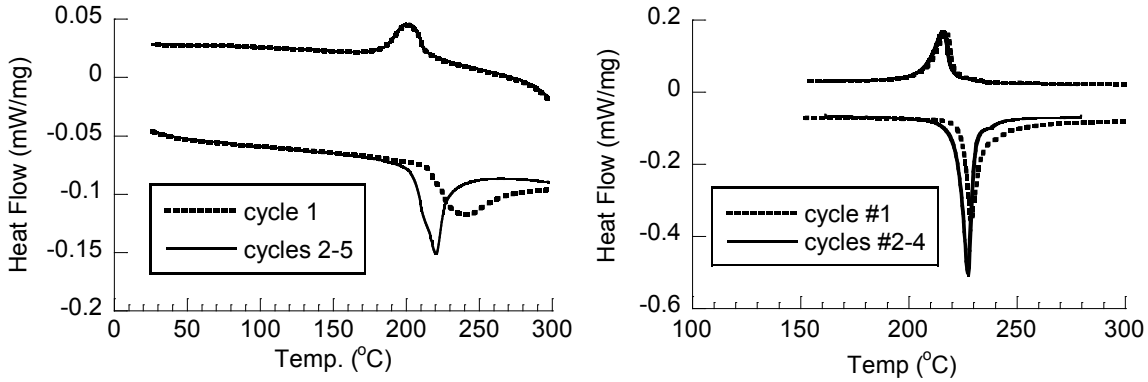

(b) 16.0%Pt (nominal)

(c) 16.5%Pt (nominal)

Figure 2- DSC traces for select cast plus homogenized Ni-Ti-Pt samples.

Table I
Transformation Temperatures of Three Selected Ni-Ti-Pt alloys

Alloy (at%Pt)	M_s (°C)	M_f (°C)	A_s (°C)	A_f (°C)
15.5	206	179	202	222
16.0	213	187	204	226
16.5	219	207	222	231

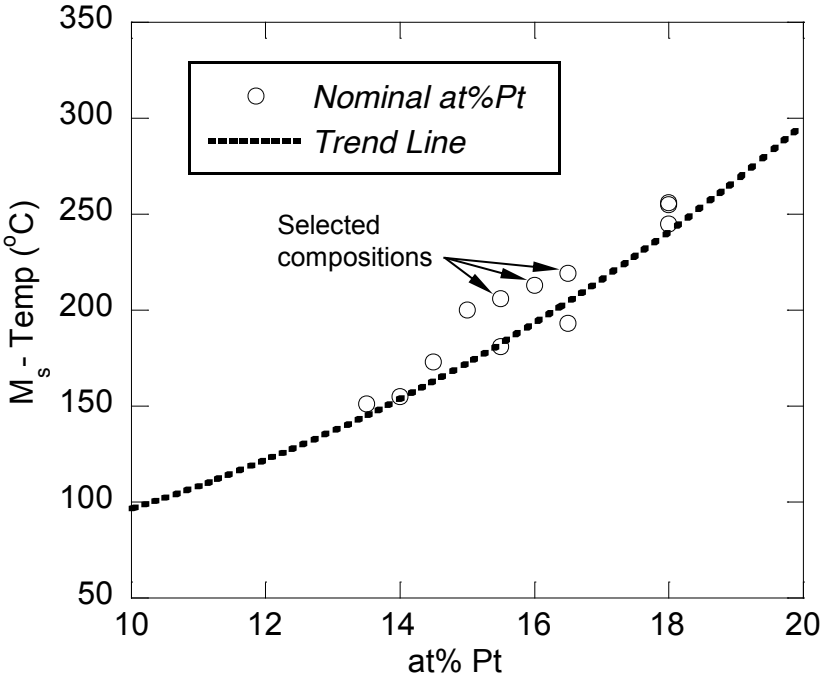

(a)

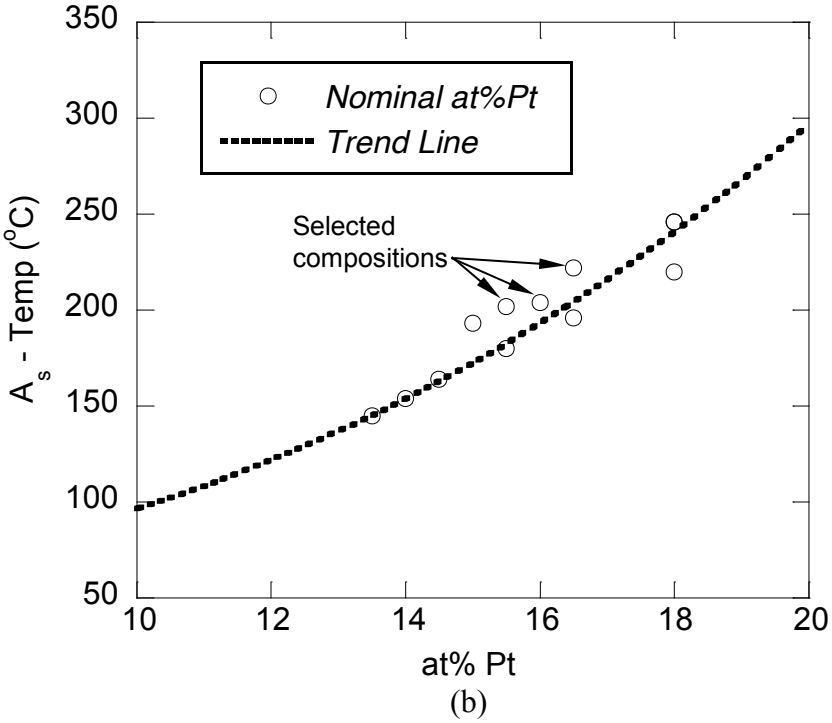

(b)

Figure 3- Transformation temperatures vs. nominal Pt content, (a) M_s and (b) A_s. Both are compared to the M_s trend line vs. at% Pt for Ni-Ti-Pt alloys, taken from previously reviewed results. [1-3, 21]

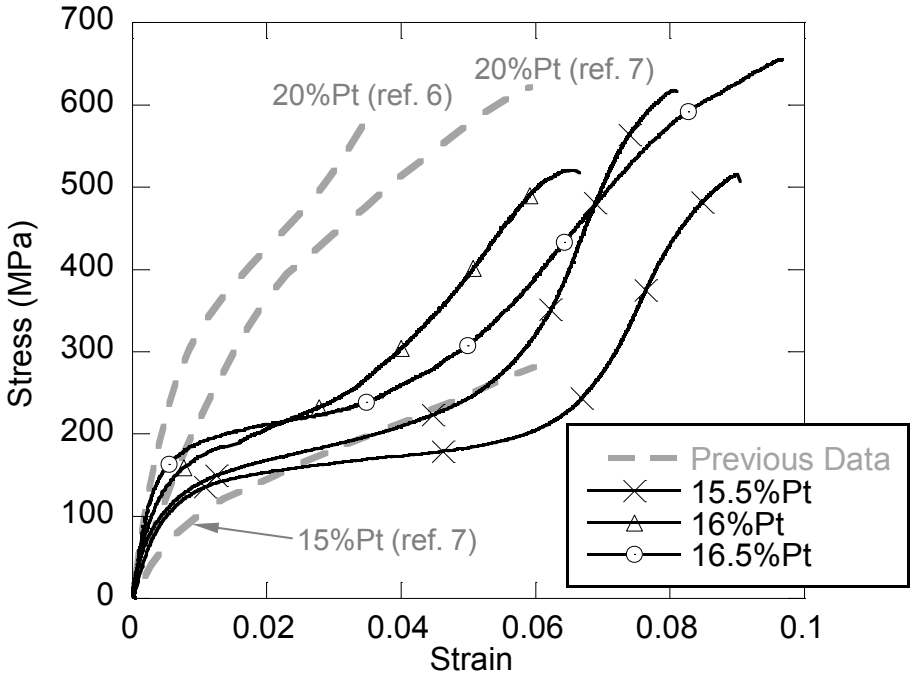

(a)

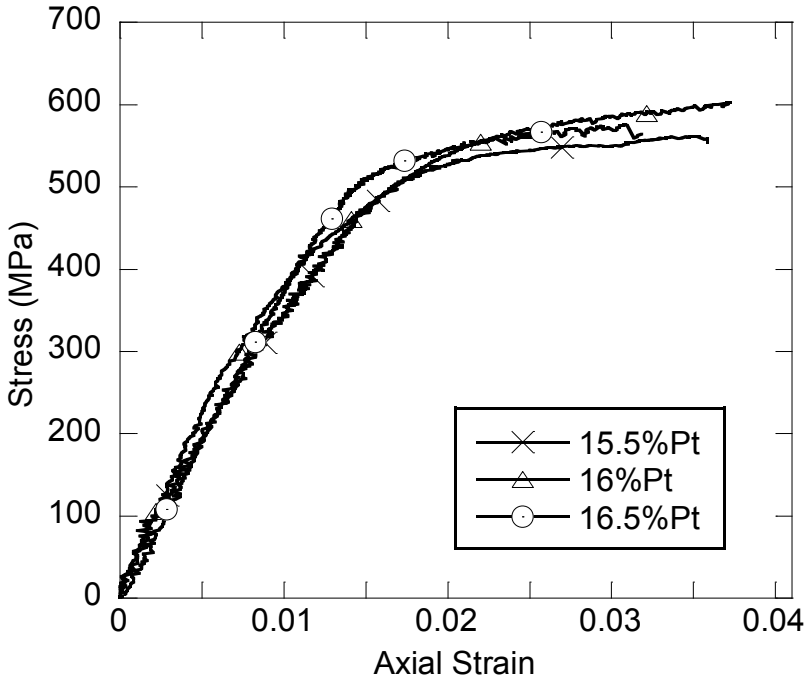

(b)

Figure 4- Tensile Stress-Strain response of Ni-Ti-Pt Shape Memory Alloys. (a) Room Temperature and (b) 275°C.

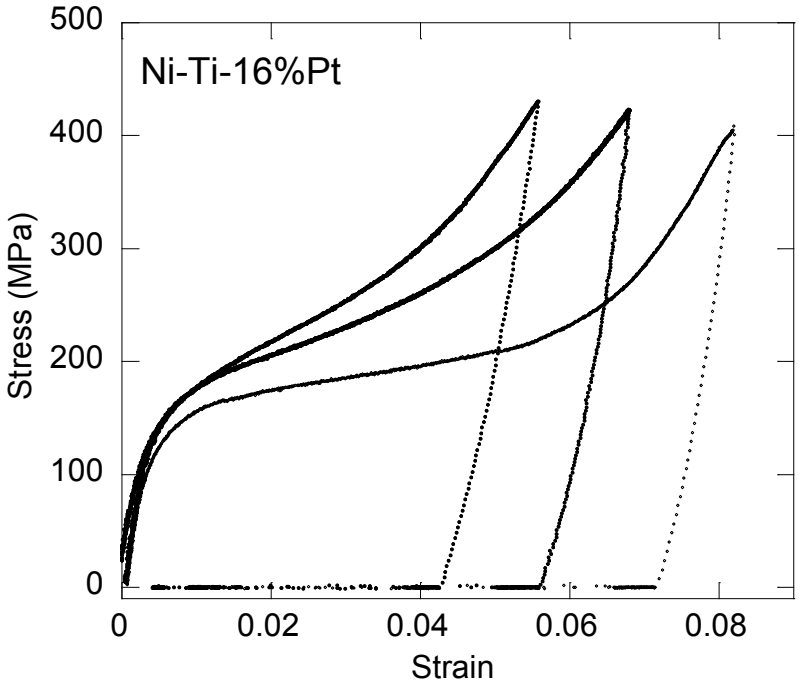

(a)

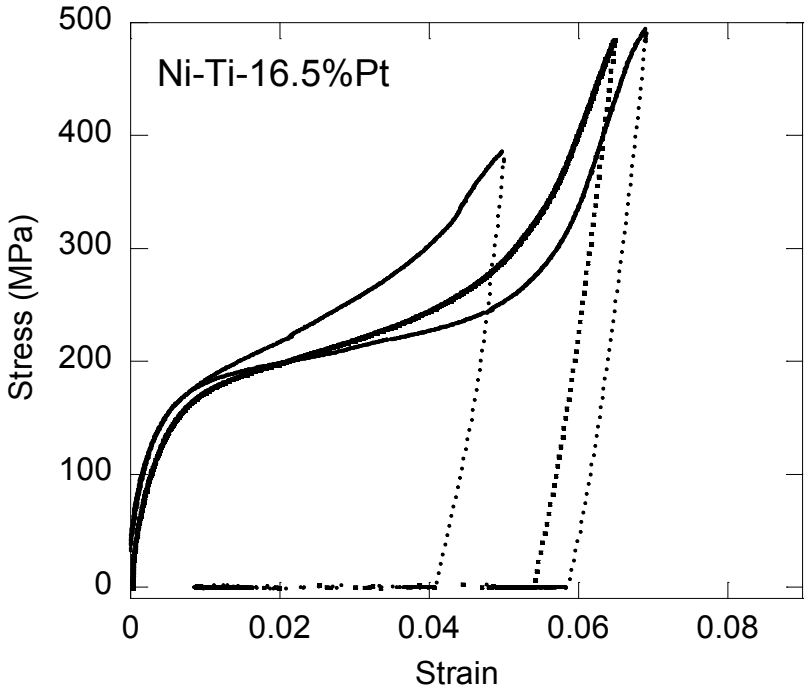

(b)

Figure 5. Variability of room temperature tensile stress-strain response observed using subscale samples (a) Ni-Ti-16%Pt and (b) Ni-Ti-16.5%Pt.

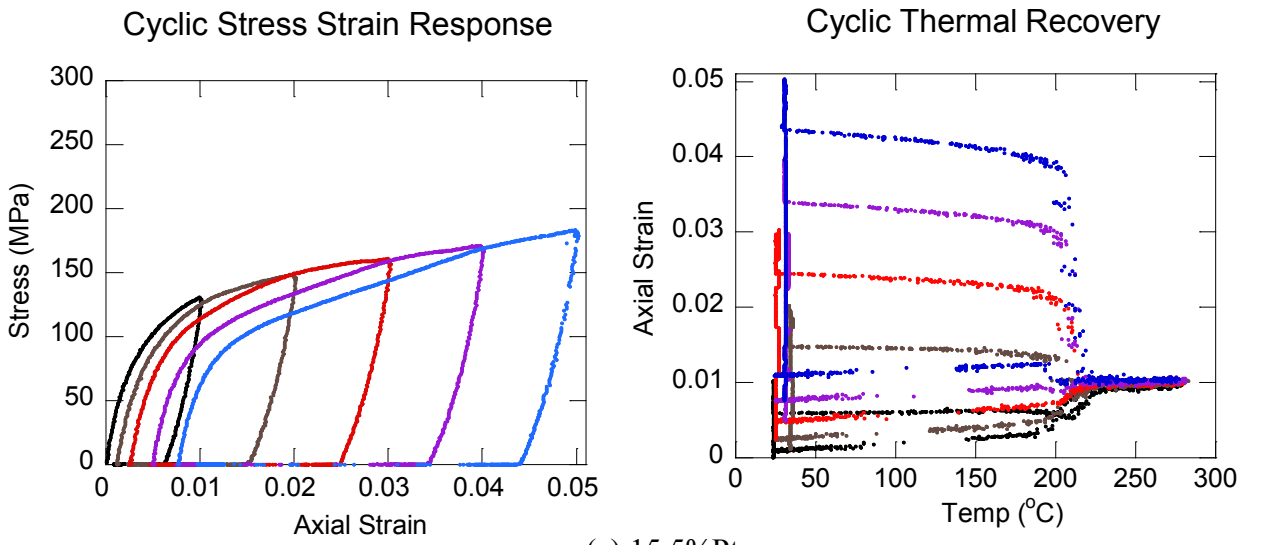

(a) 15.5%Pt

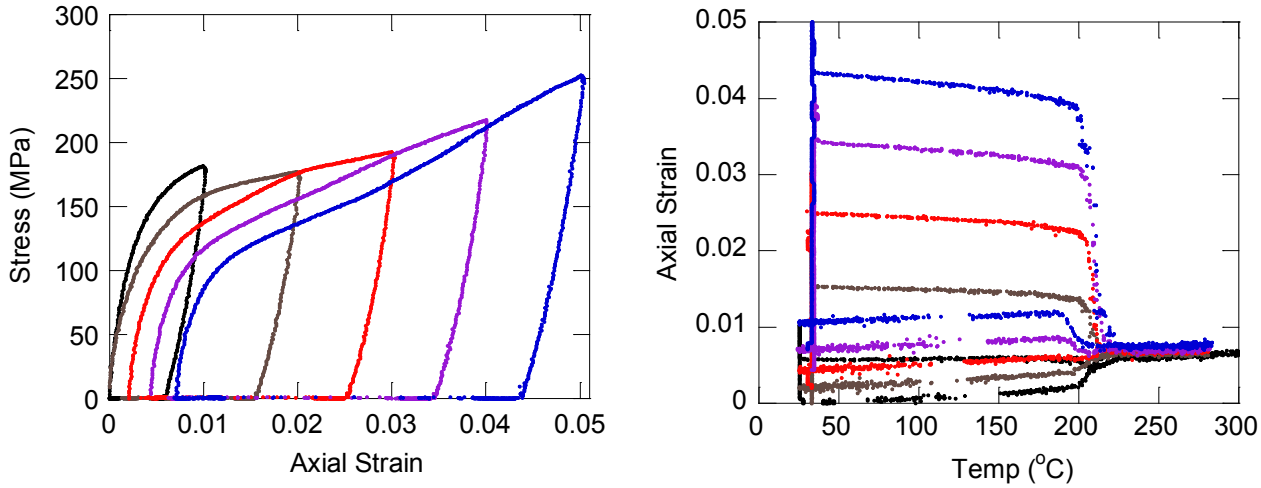

(b) 16.0%Pt

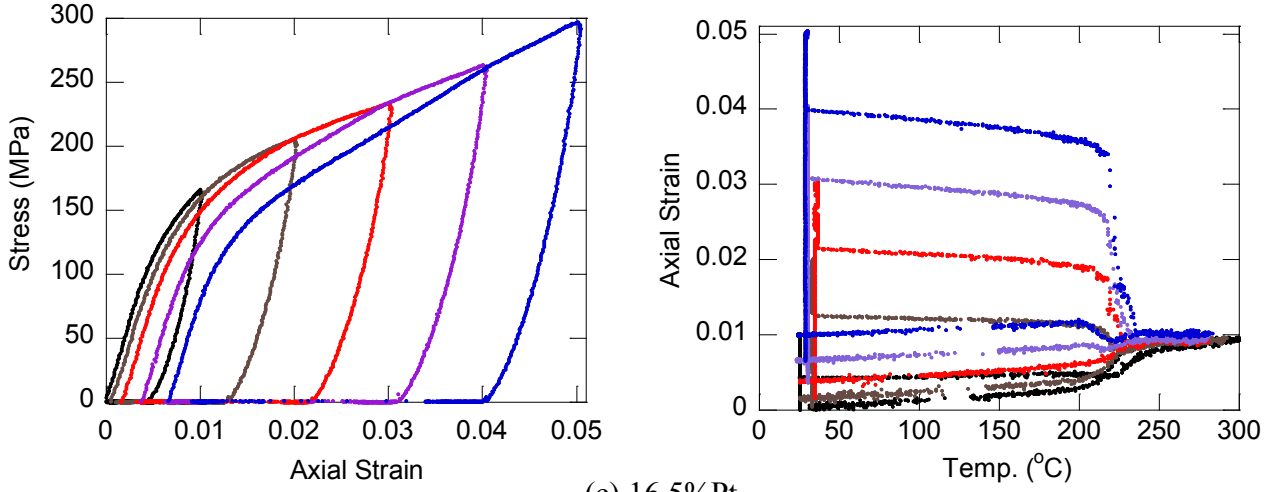

(c) 16.5%Pt

Figure 6. Stress-Strain-Temperature behavior of the Ni-Ti-Pt SMAs prestrained at room temperature to 1% - 5% strain and thermally recovered above A_f.

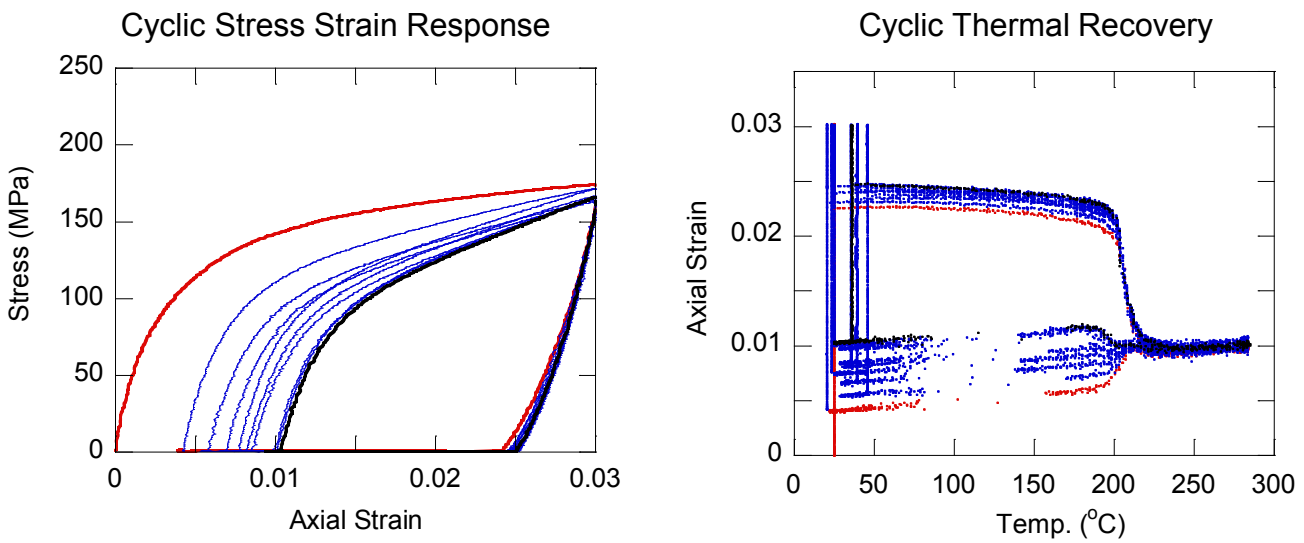

(a) 15.5%Pt

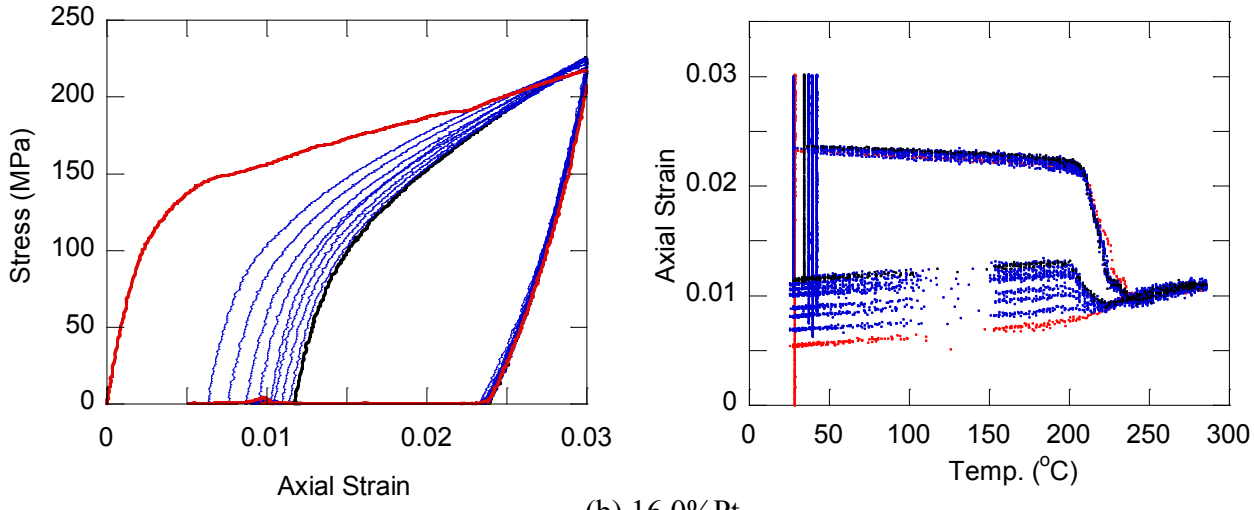

(b) 16.0%Pt

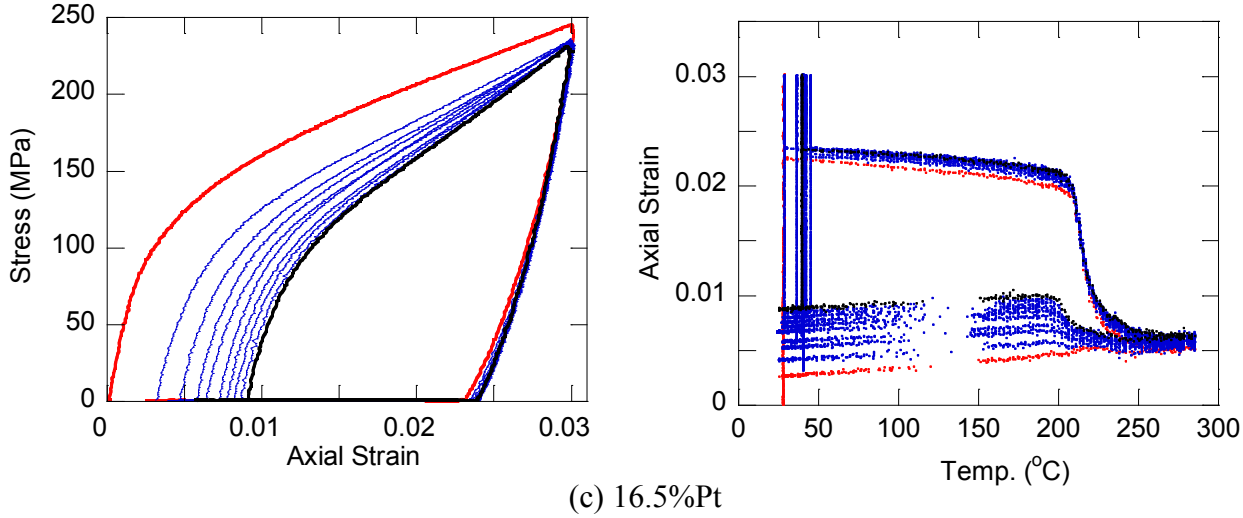

(c) 16.5%Pt

Figure 7. Cyclic Stress-Strain- Temperature results for Ni-Ti-Pt SMAs prestrained to 3% at room temperature and thermally recovered above A_f (for 10 cycles).

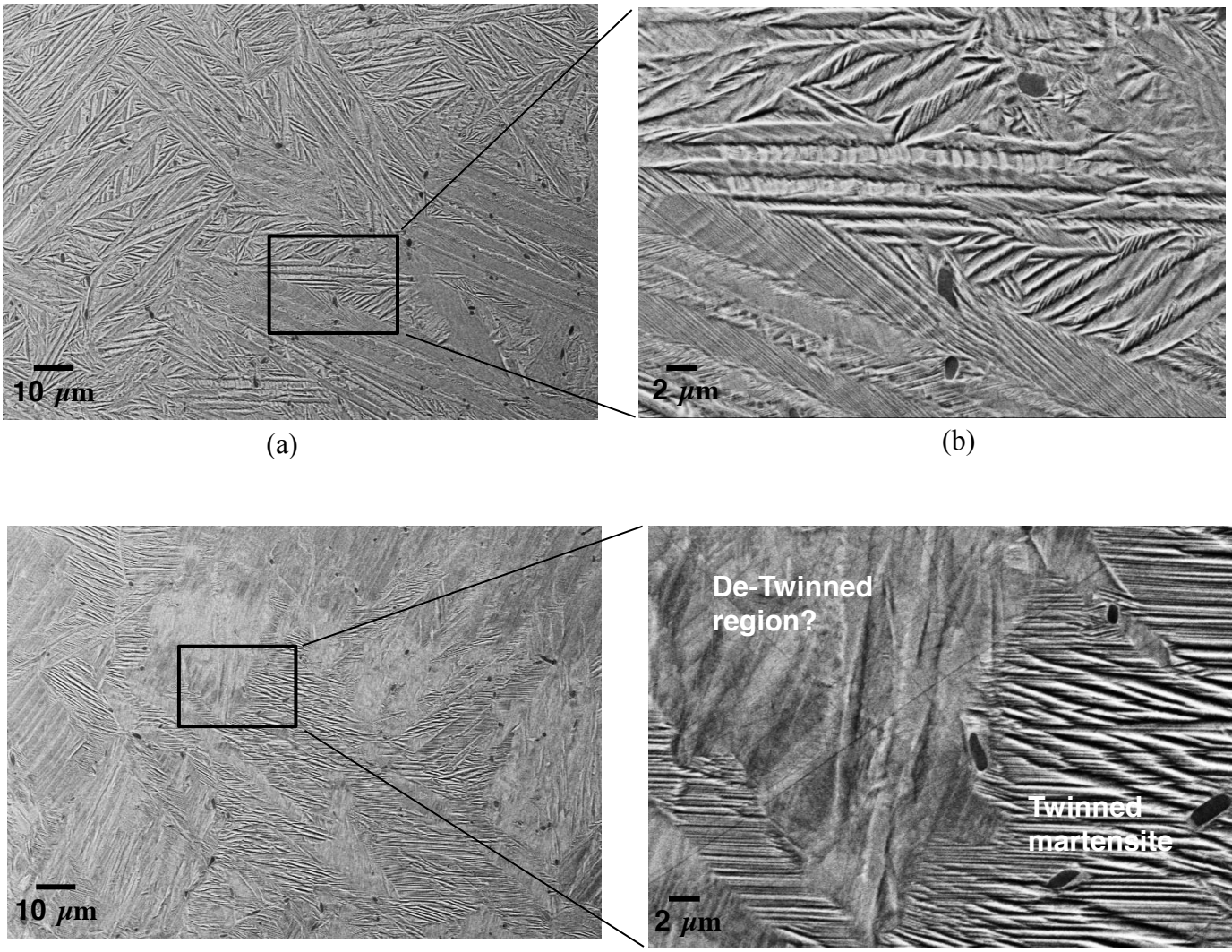

Figure 8. SEM backscatter photomicrographs of a 15.5% Pt tensile specimen in the (a,b) grip section and (c,d) center of the gage section at relatively low (a, c) and higher magnifications (b, d).

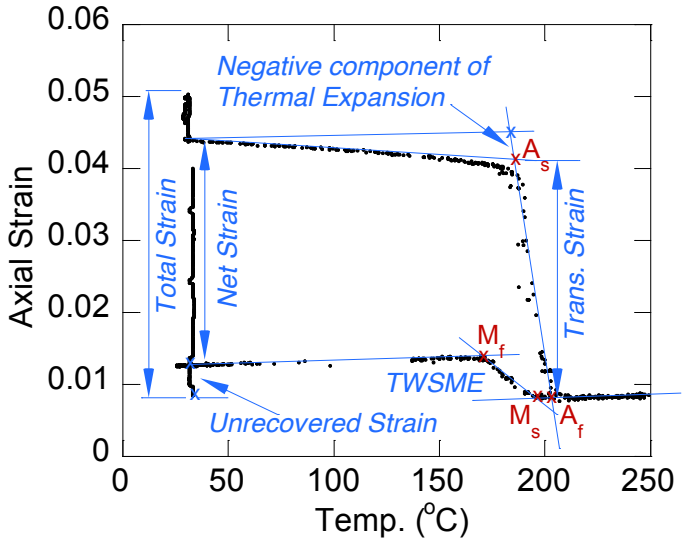

(a) Cycle 5- Ni-Ti-16%Pt shape recovery test (1%-5%)

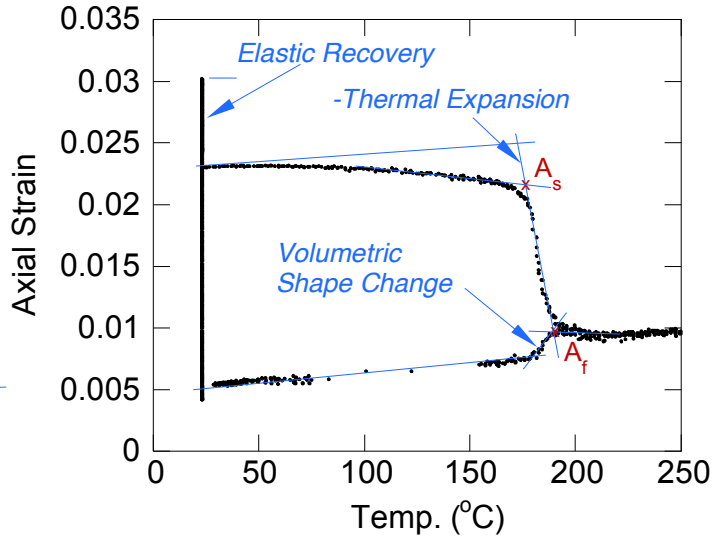

(b) Cycle 2- Ni-Ti-15.5% cyclic 3% test

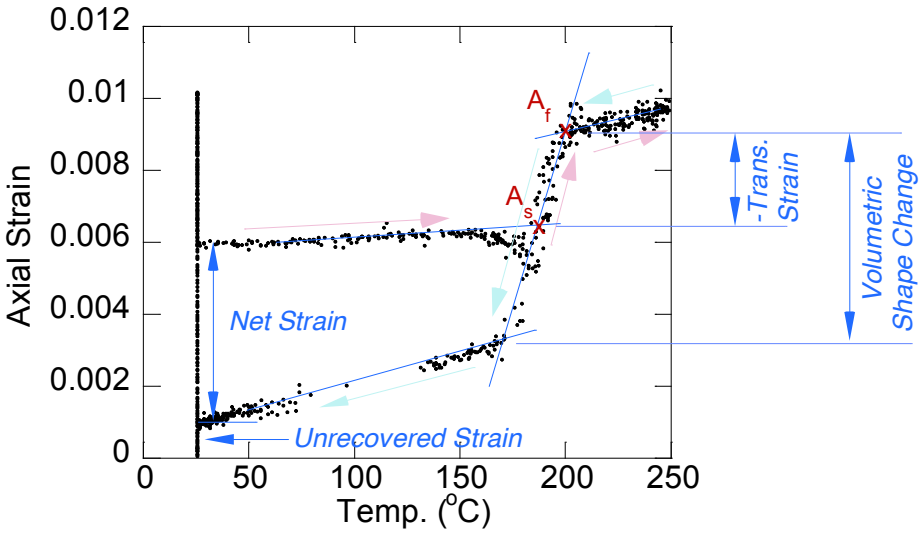

(c) Cycle1- Ni-Ti-15.5%Pt thermal recovery test (1%-5%)

Figure 9- Three examples of strain-temperature response during thermal recovery of Ni-Ti-Pt alloys and the type of strain measurements extracted from the plots. Note that the range in strains along the Y-axis is different in each case.

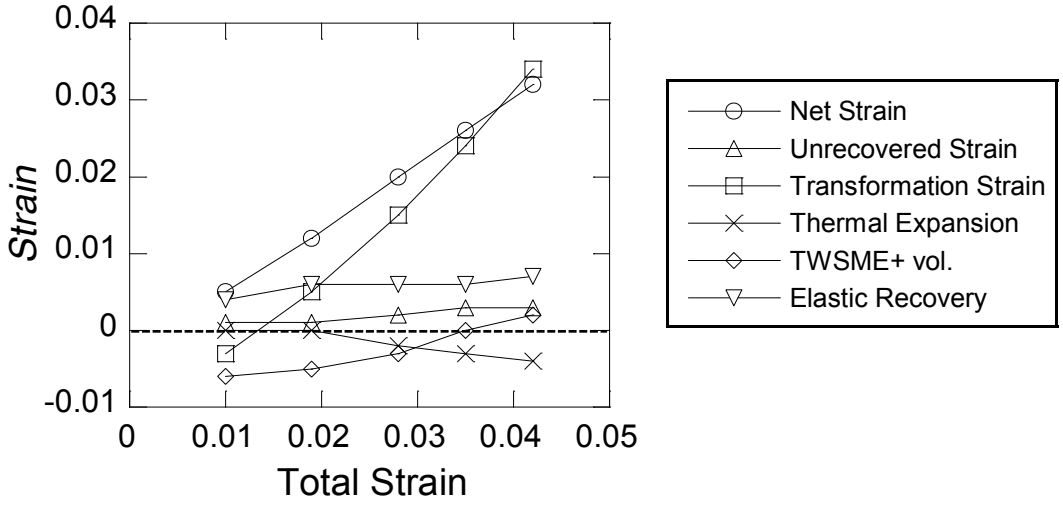

(a) 15.5%Pt

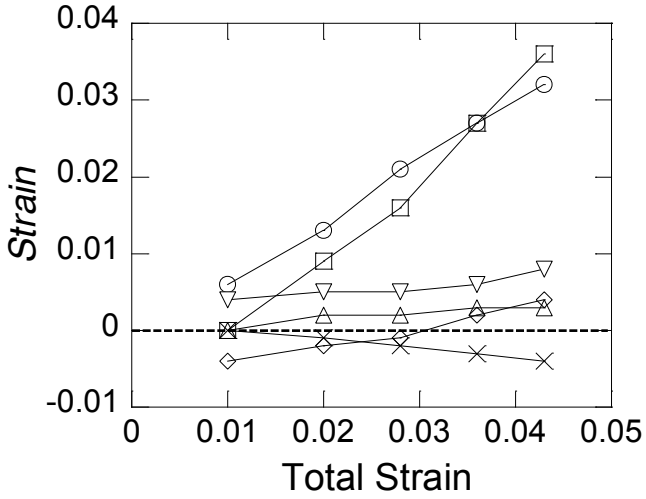

(b) 16.0%Pt

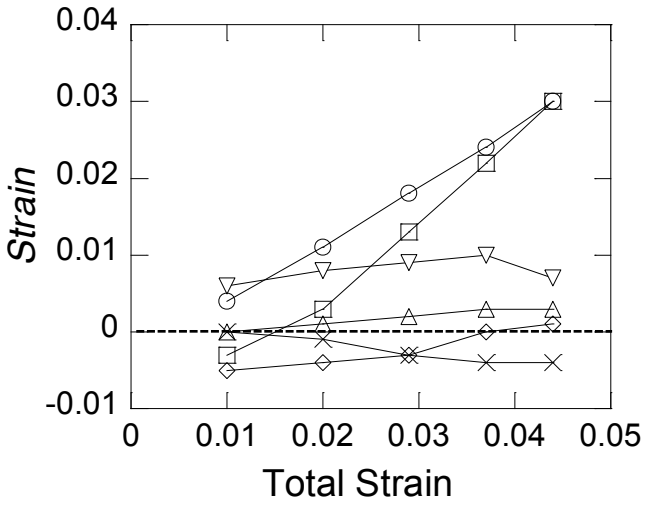

(c) 16.5%Pt

Figure 10- Summary of accumulated strain measurements as a function of total strain extracted from the 1%-5% strain thermal recovery experiments on each of the 3 Ni-Ti-Pt SMA's investigated.

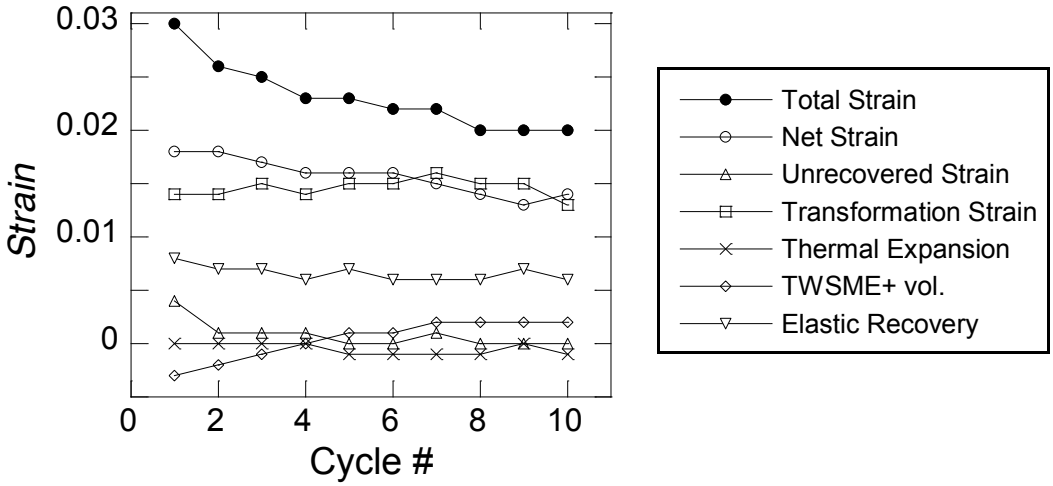

(a) 15.5%Pt

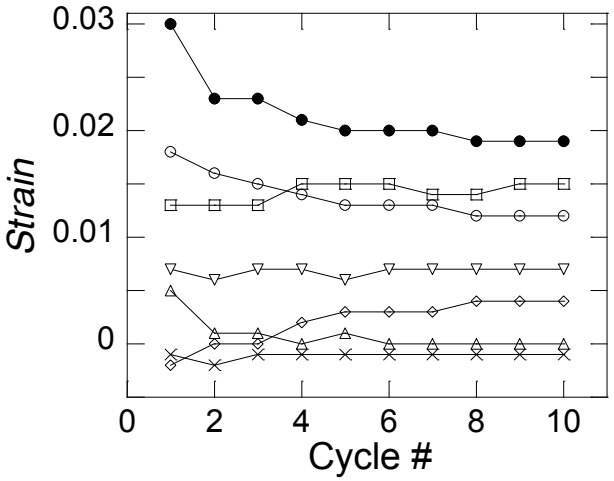

(b) 16.0%Pt

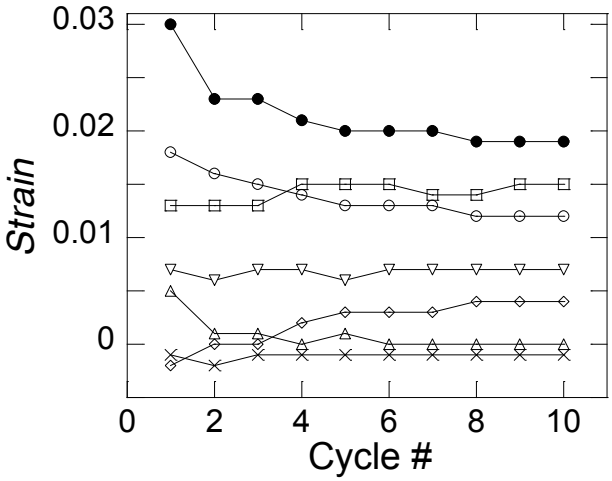

(c) 16.5%Pt

Figure 11 - Summary of accumulated strain measurements per cycle extracted from the cyclic experiments to 3% strain on each of the 3 Ni-Ti-Pt SMA's investigated.